Highly Compact Array MIMO Module for EMI Immune 5G Wireless Communications

Hyunho Cho, Woosol Lee and Yong-Kyu Yoon
Multidisciplinary nano and Microsystems Lab, University of Florida, Gainesville, FL, USA
Hyunho.Cho@ufl.edu, leewosol@ufl.edu, ykyoon@ece.ufl.edu

***Abstract*— A highly compact MIMO array antenna module with electromagnetic interference (EMI) immune capability is designed, implemented, and characterized for secure 5 GHz Wi-Fi applications. The size of the array antenna is greatly reduced by shrinking the gap between array elements to 2 mm ($0.033\lambda_0$). The mutual coupling between array elements is effectively suppressed by adding diagonally placed meander-line (ML) ring resonators under each element without degrading antenna gain and directivity performance. Compared with a conventional 2 x 2 array antenna module, the demonstrated 2 x 2 one shows 65% area reduction. The resonant frequency of the fabricated structure matches well with the target frequency. The feeding locations of the patch elements are optimized for a symmetric design. A mutual coupling reduction of more than 13 dB has been demonstrated.**

***Keywords*— electromagnetic interference, antenna array, MIMO, mutual coupling**

I. Introduction

Multiple-input and multiple-output (MIMO) antenna systems have been drawing great attention for a hardware security feature such as an anti-jamming signal function and high electromagnetic interference (EMI) immunity for both defense systems (e.g. anti-jamming radars and satellite communications) and civilian applications (e.g. IoT drones and unmanned vehicles). Drones usually employ a single patch antenna for global positioning system (GPS) communications while such a single patch is highly susceptible to intentional or unintentional external interference. For example, GPS is vulnerable to EMI as the system frequency is close to other bands such as ones for TCAS (Traffic Alert Collison & Avoidance System) and IFF (Identification Friend or Foe). Although sufficiently separated frequency bands are used to reduce EMI, it has become difficult to exclude EMI only with the frequency separation as multiple communication equipment is placed in the near proximity of drones [1]. Therefore, it is important to accommodate multiple antenna resonances to null out unnecessary interference from external signals as shown in Fig.1.

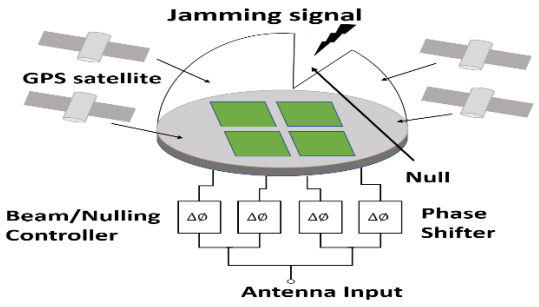

Fig. 1. Schematic of the EMI of GPS drone

An array, however, occupies larger footprint, which negatively impacts on small portable and mobile applications. The size of an array antenna is mainly dictated by the distance between the elements with generally a half-wavelength or larger ($> \lambda_0/2$), by which the mutual coupling between array elements is mitigated. There are efforts to decrease the distance between array elements without increasing mutual coupling between elements and performance degradation. Cross talk reduction between array elements has been reported by placing various decoupling structures between antenna elements [2–4].

Different from other approaches, in this work, we present a unique decoupling architecture to suppress mutual coupling. Narrow and slim ring resonator structures are diagonally placed underneath patch elements, enabling to further reduce the gap between array elements while the mutual coupling between array elements is greatly suppressed and antenna radiation performance is preserved.

II. Design of Decoupling Structure and Array

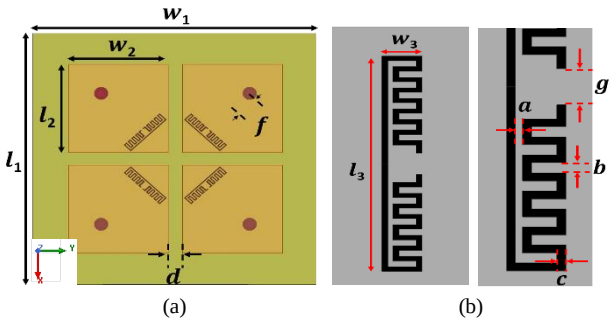

Fig. 2. Configuration of the 2 x 2 patch array module with diagonally placed 4 meander-line (ML) slots on the ground plane: (a) top view (ML slots on the ground) (b) a magnified ML slot.

Table 1. Dimensional parameters of the resonators and patches

Parameter	Value(mm)	Parameter	Value(mm)
l_1	40	a	0.16
w_1	40	b	0.2
l_2	14	c	0.16
w_2	14	d	2
l_3	7.06	f	2.4
w_3	1.39	g	0.36

Fig. 2 shows the configuration of the 2x2 patch array antenna with diagonally placed 4 meander-line (ML) slots. The structure is designed on a printing circuit board (PCB, FR-4) with a dielectric constant of 4.4 and a loss tangent of 0.02. The distance between patches is 2mm ($0.033\lambda_0$) which is much smaller than that of a conventional patch array with a typical

separation of $0.5\lambda_0$. Be noticed that this architecture places the feeding point of each patch on the diagonal axis of the patch to realize a symmetric design. The symmetric design of the array antenna provides good impedance matching capability than other architectures. This architecture enables to suppress EMI from other communication equipment using neighboring frequency bands.

The ML slot is designed to operate as a band-stop filter that blocks the surface wave currents, thereby providing isolation improvement between the patch elements at the operating frequency. The ML slots are etched from the ground plane. The compact design of the ML slots can be realized by accommodating multi-turn meander slots. Each design parameter of the ML slots is carefully optimized to have a compact size of ML slots while maintaining radiation resonance at a target frequency. The detailed dimension of the ML slots is shown in Fig. 2 (b). The simulated insertion loss (S21) of the ML slot unit cell is shown in Fig 3. The insertion loss more than 25 dB has been achieved at 5 GHz with good isolation. It is observed that the overall size of the ML slot is reduced as the number of turns is increased. Full 3D structure simulation has been performed by using a high frequency structure simulator (HFSS, ANSYS Inc.).

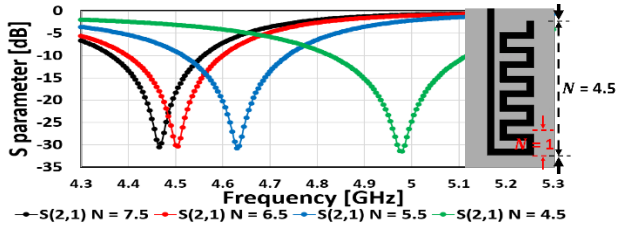

Fig. 3. Simulated insertion loss (S21) of the ML slot according to the number of folded ML slots. Inset shows how to calculate the parameter N.

III. Simulation and Measurement Results

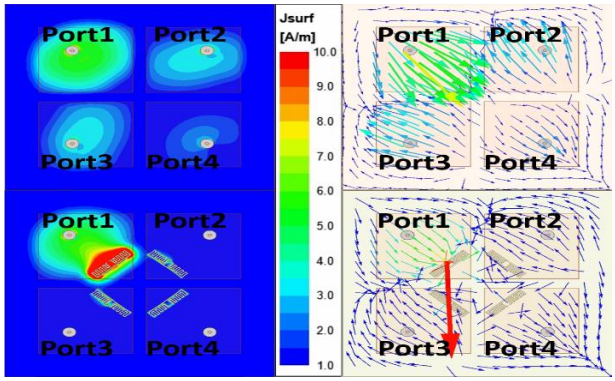

Fig. 4. Configuration of current distribution and current flow without ML slots (top left and right) and with ML slots (bottom left and right).

Fig. 4 shows the current distribution and current flow of the 2 x 2 patch array with and without the ML slots where port 1 is excited and port 2, 3, 4 are terminated with 50 ohms. From port 1, high concentration of the surface currents appears on the port 2, 3, 4 without ML slots due to the strong mutual coupling (top left and right plots). On the other hand, less current concentration has been observed on the other port with ML slots, while high current distribution is shown on the ML slots which indicates the surface current flow is blocked by ML slots between patches. The simulated current distribution and current flow results show that isolation improvement can be achieved by inserting the ML slots under the patches.

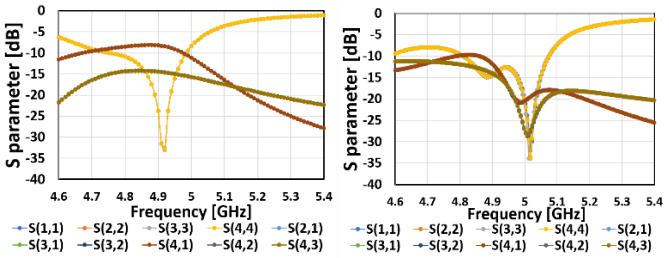

(a) (b)

Fig. 5. Simulated return loss and insertion loss of the 2 x 2 patch array: (a) without ML slots and (b) with ML slots.

Fig. 5 shows the return loss and insertion loss without/with ML slots. Since the patches are designed symmetrically, there is no resonant frequency mismatching between patches. The test results are summarized in Table 2, where the enhancement of mutual coupling reduction for the one with ML compared with the one without ML is between 11.11dB and 13.26dB.

Table 2. Comparison of simulated S parameter

	Without ML	With ML	Improvement
Resonant frequency	4.92GHz	5.02GHz	N/A
S11(dB)	32.94	32.06	-0.88
S22(dB)	32.49	33.47	0.98
S33(dB)	33.03	34.04	1.01
S44(dB)	32.77	33.78	1.01
S21(dB)	14.56	27.82	13.26
S31(dB)	14.58	27.36	12.78
S41(dB)	8.35	19.54	11.19
S32(dB)	8.35	19.46	11.11
S42(dB)	14.58	27.62	13.04
S43(dB)	14.59	27.18	12.59

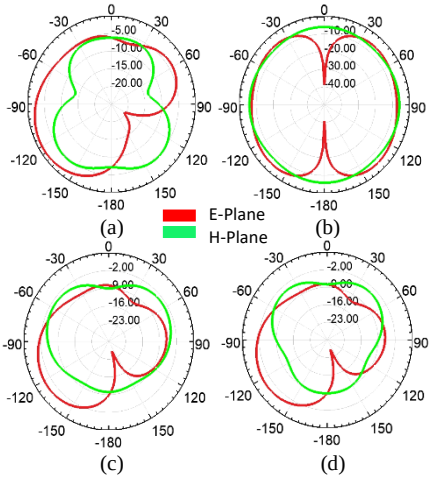

Fig. 6. Radiation pattern of E-Plane and H-Plane: (a) Case1 (b) Case2 (c) Case3 (d) Case4

Table 3 Classification of case 1 - 4

	Port1		Port2		Port3		Port4	
Case1	1V	0°	0V	0°	0V	0°	0V	0°
Case2	1V	0°	1V	0°	1V	0°	1V	0°
Case3	1V	90°	1V	180°	1V	180°	1V	0°
Case4	2V	90°	1V	180°	1V	180°	0.5V	0°

Table 4. Comparison of antenna performance

	Peak Directivity	Peak Gain	Radiation Efficiency	Front-Back-Ratio
Case1	3.17	0.78	0.246	1.91
Case2	1.83	0.51	0.277	1.28
Case3	3.78	0.91	0.24	17.66
Case4	4.93	1.22	0.25	8.92

Fig. 6 represents the E/H-plane radiation patterns of the antenna according to four different operating cases from case 1 to 4. The radiation pattern can be controlled by changing the amplitude and phase of each power source. Especially, case 2 shows the omni-directional radiation pattern like dipole antenna which has the nulls to the vertical direction (0°, 180° in E-Plane) when the amplitude and phase are all the same. Table 4 shows the antenna performance case by case, while showing the best performance for case 4. The radiation efficiency can be improved by using the substrate which has a low loss value.

IV. FABRICATION

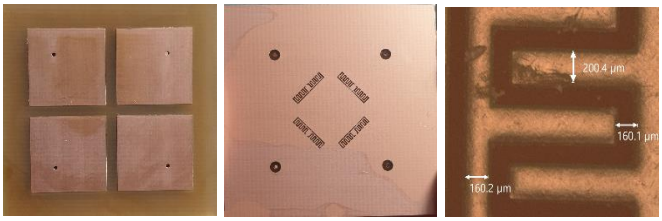

(a) (b) (c)

Fig. 7. Photographs of a fabricated 2 x 2 patch array with ML slots on the ground plane: (a) top view (b) bottom view with ML slots (c) a magnified ML slots

Fig. 7 shows a fabricated 2 x 2 patch array with ML slots. Milling machine is used to cut the patch on top of the substrate and photolithography is used to pattern the narrow ML slots on the ground plane. Fig. 7(c) shows an etched ML slot whose dimension is very close to the designed specification.

V. MEASUREMENT RESULTS

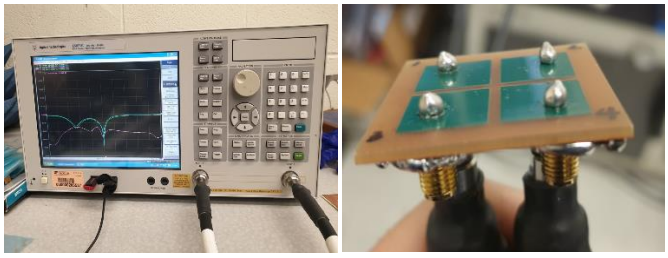

(a) (b)

Fig. 8. Photographs of (a) vector network analyzer (VNA) (b) a complete device with connectorized feeding points and soldered patches

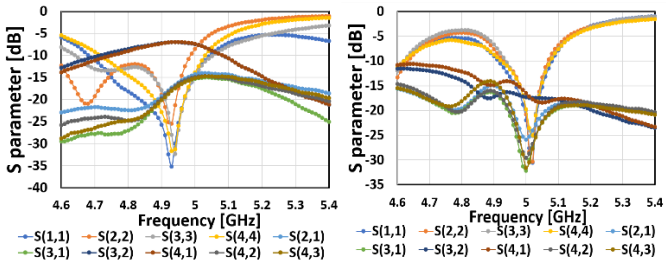

(a) (b)

Fig. 9. Measured S parameter (a) without ML slots (b) with ML slots

Fig. 8 shows the photographs of antenna measurements with vector network analyzer (VNA). Fig. 9 shows the measured S parameter of the 2 x 2 patch arrays without/with ML slots. With ML slots diagonally placed under the patches, the entire insertion loss is enhanced at the target frequency, as shown in Table 5. The measured results show good matching with the simulation results shown in Fig. 5. There is no mismatching resonant frequency between fabricated patches because of the symmetric design, but the overall 10dB bandwidth of resonant antennas decreased.

Table 5. Comparison of the measured S parameter

	Without ML	With ML	Improvement
Resonant frequency	4.93GHz	5.02GHz	N/A
S11(dB)	35.18	31.42	-3.76
S22(dB)	25.48	35.46	9.98
S33(dB)	32.32	25.62	-6.7
S44(dB)	31.66	25.14	-6.52
S21(dB)	17.32	24.66	7.34
S31(dB)	17.97	28.68	10.71
S41(dB)	7.02	17.45	10.43
S32(dB)	7.02	17.48	10.46
S42(dB)	17.59	27.74	10.15
S43(dB)	18.06	29.14	11.08

Table 6. Comparison of the proposed antenna to other state-of-the-art antennas

Year	Separation	Improv.	Antenna Size	RF. shift
2018[2]	$0.99\lambda_0$	8.7dB	$3.78\lambda_0$x$4.1\lambda_0$	NR
2018[3]	$0.32\lambda_0$	NR	$1.42\lambda_0$x$1.42\lambda_0$	Shifted
2019[4]	$0.62\lambda_0$	9.5dB	$2.5\lambda_0$x$2.5\lambda_0$	Shifted
This work	$0.033\lambda_0$	7.3 – 11.1dB	$0.67\lambda_0$x$0.67\lambda_0$	Matched

VI. CONCLUSION

High isolation between antenna elements is realized by inserting a diagonally placed meander-line ring resonator on the ground plane under each patch, which maintains well MIMO antenna performance. Furthermore, the radiation pattern can be reshaped to produce nulls against EMI and jamming signals by controlling the amplitude and the phase of the power source. The symmetric design of the MIMO antenna module mitigates the impedance mismatching of the radiation resonance frequency. From this work, the most compact MIMO antenna module with EMI immunity has been demonstrated. Both milling machine and microfabrication processes are used. Performance comparison of the demonstrated antenna module

with other state-of-the-art 2 x 2 array antennas shows no degradation of radiation or controlled beam capability.

REFERENCES

[1] Kim, Choon-Won & Kim, Ji-Hoon & Kwon, Kyoung-Il & Chung, Deok-Cho. (2011). An efficient Method of Antenna Placement considering EMI between equipments on UAV. Journal of the Korean Society for Aeronautical & Space Sciences. 39. 987-994. 10.5139 / JKSAS. 2011.39.10.987.

[2] Alshaheen, Ahmad. (2018). Surface wave minimizing 2x2 microstrip antenna array. 10. 67-77.

[3] Xu, Kai-Da & Zhu, Jianfeng & Liao, Shaowei & Xue, Quan. (2018). Wideband Patch Antenna Using Multiple Parasitic Patches and Its Array Application With Mutual Coupling Reduction. IEEE Access. 6. 1-1. 10.1109/ACCESS.2018.2860594.

[4] Zhang, Shuai & Chen, Xiaoming & Pedersen, G.F.. (2019). Mutual Coupling Suppression With Decoupling Ground for Massive MIMO Antenna Arrays. IEEE Transactions on Vehicular Technology. PP. 1-1. 10.1109/TVT.2019.2923338.